

# Reconstruction of Blood Vessels from Neck CT Datasets using Stable 3D Mass-Spring Models

Jana Dornheim<sup>1</sup>, Dirk J. Lehmann<sup>1</sup>, Lars Dornheim<sup>1</sup>, Bernhard Preim<sup>1</sup> and Gero Strauß<sup>2</sup>

<sup>1</sup>Otto-von-Guericke University of Magdeburg, Germany

<sup>2</sup>ENT University Hospital of Leipzig, Germany

---

## Abstract

*Preoperative neck dissection planning benefits from a smooth, organic visualization of the main blood vessels of the neck, in particular the carotid artery and jugular vein. While most reconstruction techniques for vasculature are designed for segmenting the complete vessel tree, our goal is to isolate these specific blood vessels of the neck from the CT dataset, and to exclude irrelevant vasculature from the visualization.*

*Pure threshold- and iso value-based reconstruction techniques do not allow such a selective segmentation and often lead to undersegmentation at the lower parts of the blood vessels, due to inhomogeneous contrast agent diffusion. In order to avoid staircase artifacts in the visualizations of the reconstructed vascular structures, a subvoxel accuracy of the reconstruction technique is also required.*

*We present a model-based reconstruction technique to isolate blood vessels from neck CT datasets using Stable 3D Mass-Spring Models. The results can be visualized directly without staircase artifacts. The interaction needed for the reconstruction is reduced substantially to only a few clicks along the blood vessels.*

*The presented method was evaluated with 30 blood vessels from 14 CT datasets of the neck and could be shown to be accurate, while leading to smooth visualizations of the neck blood vessels.*

Categories and Subject Descriptors (according to ACM CCS): I.4.6 [Image Processing and Computer Vision]: Segmentation

---

## 1. Motivation

Neck dissections are carried out in the context of tumor therapy in the head and neck region, in order to eliminate lymph node metastases. For the preoperative planning of this surgery, a visualization and quantification of the neck blood vessels is often required [CDP\*06]. The goal is to detect abnormalities of the vessels like stenosis or occlusion due to compression or infiltration by the tumor, and to assess the complex spatial relationship of metastasis to the vascular structure. This demands a reconstruction of the relevant blood vessels from CT datasets of the neck, which can be used for visualization and quantification.

For the planning of neck dissections, specific blood vessels are relevant for the therapeutic decision (especially the carotid artery and jugular vein), while other parts of the vessel tree are less essential for the planning. We therefore demand an efficient interactive extraction technique which allows the user to reconstruct specific blood vessels from

the dataset, while irrelevant branches of the vessel tree are ignored. Additionally, accuracy and a smooth visualization without distracting staircase artifacts are required for an efficient and reliable blood vessel assessment.

So far, the large majority of existing approaches to blood vessel reconstruction is rather general. However, blood vessels of the neck exhibit the following characteristics enabling and requiring a more specific reconstruction technique:

1. Most blood vessels in the neck are primarily parallel to the body axis, which leads to nearly circular cross sections and only slight deviations of the blood vessels centerline from the direction of the body axis.
2. The blood vessels in the focus of this paper have few bifurcations, in most cases only the main bifurcation of the A. carotis and V. jugularis needs to be taken into account.
3. For contrast-enhanced blood vessels, the outline exhibits a strong gradient, which may however be interrupted at

curvature points or where an adjacent high-contrast structure touches the blood vessel.

4. The interior gray value is locally homogeneous, but may change slightly from slice to slice so that one specific gray value range across the whole vessel cannot be assumed.

We therefore present a model-based reconstruction technique dedicated to vascular structures in the neck region, and to the specific requirements of therapy planning, which include smooth visualizations without staircase artifacts.

## 2. State of the Art

A good overview on the field of blood vessels segmentation is given by [KQ04]. As their survey shows, most blood vessel segmentation techniques result in a binary classification of the voxels of the dataset. Typical examples are the use of a sophisticated watershed transformation [HP03], region growing [SPSP02], statistical classification or neural networks. The most serious drawback of all these voxel-based segmentation techniques is the reduction of the gray scale to binary information, leading to staircase artifacts when an iso surface is created directly from the binary mask.

To overcome this drawback, much research has been directed towards smoothing techniques in order to improve the resulting visualizations [BKP07]. However, smoothing can only be performed at the expense of accuracy and is especially problematic for elongated structures such as blood vessels. Model-based visualization techniques have been developed to achieve smoother visualizations by model assumptions, e.g. a circular cross-section [OP05, HPSP01]. These techniques have been designed for the visualization of complex vascular trees, in which the cross-section of individual vessels is less essential. For neck dissection planning however, the shape of the blood vessel's cross section is an important indicator for tumor infiltration and must therefore be visualized correctly.

Sophisticated surface reconstruction techniques operating on binary segmentation masks are Constrained Elastic Surface Nets [Gib98] or MPU implicits [SNB\*08], which lead to smoother reconstructions of surfaces from binary segmentation masks, resulting from a preceding voxel-based segmentation technique. However, when the loss of information by binarisation can be avoided, such a reconstruction technique is not needed.

Shape model-based segmentation techniques for blood vessels are often based on generalized cylinders [FVHO04, FNN\*00]. One recent example is the vessel crawler [MH06]. However, these techniques have not been evaluated with clinical CT datasets, and hardly any resulting visualizations are shown.

Level sets are often applied to the segmentation of blood vessels. However, they are specifically suited for the segmentation of complex-shaped vessel trees, for which shape

model-based techniques would be inappropriate. The prevention of leaking with level sets is based on the size of branching vessels, rather than on semantics. In favor of computation times, most approaches are implemented using fast marching, which again leads to a binary segmentation mask. In [RTT06], levels sets have been applied to the segmentation of neck blood vessels without being able to prevent leaking to irrelevant branches or staircase artifacts.

## 3. Method

We employ Stable 3D Mass-Spring Models (SMSMs) [DTD05] for the segmentation of neck blood vessels, which enable an explicit modelling of the blood vessel characteristics, and achieve a subvoxel accuracy due to the polygonal representation.

SMSMs extend conventional mass-spring models by the use of an additional internal force called *torsion force*, which helps to maintain shape stability. The external model forces of an SMSM are created by *sensors* at the mass points, dragging their associated masses towards specific image information, like gradients or a specific gray value range.

For the segmentation of neck blood vessels, the vessels' shape coherency across the slices should be exploited to make the segmentation more robust. Therefore, instead of using a purely slice-wise approach, information from the neighbouring slices should be used during the segmentation of each slice. On the other hand, a complete three-dimensional model is not appropriate, as the global shape of the blood vessels varies across patients, and a constant gray value range across one vessel can rarely be found.

We therefore decided to use SMSMs for the blood vessel segmentation in the following three-stage process:

1. The blood vessel's center line is created from a set of markers the user places inside the target blood vessel.
2. Along the center line, the blood vessel is segmented slice-wise with a cylindrical SMSM, which segments the vessel locally, but uses knowledge from neighbouring slices for robustness.
3. The results of all slices are connected to the final reconstruction result.

These stages are now described in detail.

### 3.1. Generation of the Blood Vessel's Centerline

To specify the target blood vessel, the user places a set of markers in the center of the blood vessel (Fig. 1(a)). The minimum number is one marker for each end point of the blood vessel, plus one marker for each bifurcation. For curved vessels, additional markers should be placed at points of high curvature.

All markers are then connected in the order of their  $z$  coordinate by interpolation with cubic B-splines. Due to the

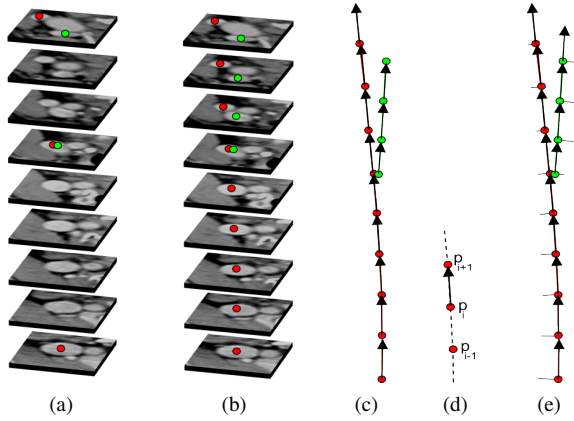


**Figure 1:** Creation of the blood vessel's skeleton line: (a) markers placed by the user; (b) interpolated markers for intermediate slices; (c) raw skeleton line; (d) calculation of the inclination vector; (e) annotated skeleton including inclination directions and initial model radii

body axis parallelity, this results in one marker per slice and branch (Fig. 1(b)). When a bifurcation exists in the target blood vessel, a separate skeleton line is created for each branch (Fig. 1(c)).

After the skeleton line has been generated, the inclination vector of the blood vessel at each marker position, as well as the initial radius and local gray value range for the cylindrical model generation are computed. The inclination vector  $\vec{g}_i$  at the skeleton point  $\vec{p}_i$  is computed from the neighbouring skeleton points via  $\vec{g}_i = \frac{\vec{p}_{i+1} - \vec{p}_{i-1}}{\|\vec{p}_{i+1} - \vec{p}_{i-1}\|}$  (Fig. 1(d)). The radius and the local gray value range for the model initialization are computed by the following ray casting procedure:

1. Starting from the centerpoint  $\vec{p}_i$  of the current slice,  $n$  rays are cast in all directions at equidistant angles. For each ray, the intersection point with the blood vessel contour is estimated as the first point on the ray, for which the homogeneity criterion  $H: |f(\vec{p}) - f(\vec{p}_i)| < \mu$  (with  $f(\vec{x})$  being the average gray value in a  $3 \times 3 \times 3$  environment around  $\vec{x}$ ) is broken. At this point, we place the contour candidate  $p_{Gj}$ . (Fig. 2(a)) The parameter  $\mu$  depends on the standard deviation of the gray values at point  $\vec{p}$ , and is calculated as  $\mu = 0.638 \cdot \sigma + 43.803$ , where  $\sigma$  is the standard deviation of all gray values in the  $5 \times 5$  environment of  $\vec{p}$ . This function was determined empirically by a linear regression analysis.
2. Outliers are filtered by a statistical analysis of the  $x$ ,  $y$  and  $z$  coordinates of all contour candidates. A threshold of  $1.6 \cdot \sigma$  was used equally for all directions (Fig. 2(b)).
3. In order to correct seed points placed slightly off-center by the user, the centerpoint is moved to the centroid of all points  $p_{Gj}$ , in order to move it more towards the center of the blood vessel's cross-section. In the case of ex-

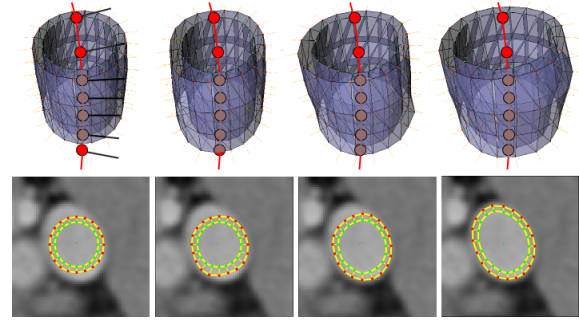


**Figure 3:** 2D and 3D view of the model adaptation process.

centric cross sections, this repositioning needs to be repeated, because necessary contour points are often eliminated by the conservative filtering of the outliers.  $n = 3$  has proved to be a sufficient number of repetitions in our experiments. The repositioning procedure has no effect on points which are already located in the centroid.

4. The ray with the shortest distance to the contour is used as the radius for the circular slice submodel. (Fig. 2(c))
5. The local gray value range of the blood vessel at the current position is estimated from an environment of  $3 \times 3 \times 3$  voxels around the skeleton point.

The described process results in an annotated skeleton line of the target blood vessel with one seed point per slice and branch, containing also the local radii, inclination directions and local gray value ranges for each skeleton point (Fig. 1(e)).

### 3.2. Slicewise Segmentation of the Blood Vessel

The annotated skeleton is used to create a cylindrical SMSM for each slice of the dataset, which is then used to segment the blood vessel in this slice. The use of a cylindrical model instead of a 1-slice circular model allows to use the context information from the neighbouring slices for more stability with respect to image artifacts, and to deal with the global inhomogeneity on the other hand. For all datasets, a number of 4 slices has been a good trade-off between stability on the one hand, and computation times as well as handling of global inhomogeneities on the other hand.

From the annotated skeleton, for each of the 4 slices the individual inclination direction and the radius are used to generate the circular submodel for this slice. It consists of a ring with radius  $r_i$  of gradient sensors modelling the strong gradient information at the blood vessel's border. A concentric second ring with radius  $r_i \cdot 0.9$  is added, consisting of intensity sensors, which represent the local homogeneous interior of the blood vessel. This layer is used to stop the model from being distracted by neighbouring structures of higher gradients, e.g. bones. Both layers are connected by

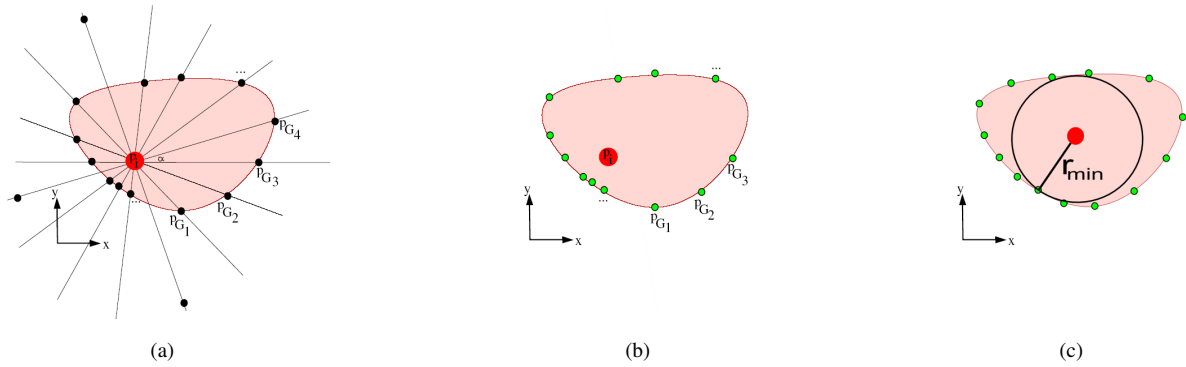


**Figure 2:** Ray casting for the calculation of the initial model radius: (a) initial contour point candidates, (b) after elimination of outliers, (c) determination of the initial model radius for the current slice

stiff springs, in order to work as a functional unit as suggested in [DSP\*07]. Both rings of one slice submodel are contained in a plane through the respective skeleton point with the normal vector of the plane being  $\vec{g}_i$ . All four slice submodels are connected by springs and faces, as shown in Figure 3.

After the cylindrical SMSM has been created, its adaptation to the dataset is started with the simulation parameters shown in Table 1. All parameters have been determined by experimentation and led to good results for all available datasets. The model motion is stopped automatically, when the movement of all masses falls below a given threshold  $\epsilon$  (see Table 1) for 5 simulation steps. Due to the use of a damping force, the model always converges and stops. The adaptation of the cylindrical model to one slice is illustrated by Figure 3.

### 3.3. Combination of the Results

The described model creation and adaptation process is carried out for all points of the skeleton line. The top and bottom slices of each cylindrical model have less influence from the neighbouring slices, and are therefore less reliable than the center slices. They are therefore discarded, while the center slices of all resulting cylindrical SMSMs are interconnected with each-other in the order of their position on the center-line (Figure 4).

The resulting mesh can be visualized directly, which leads to smooth visualizations without staircase artifacts.

### 3.4. Implementation

The described techniques were implemented using the image analysis and visualization platform MeVisLab<sup>†</sup>, and the

<sup>†</sup> <http://www.mevislab.de>

Magdeburg Shape Model Library (MSML) provided by Lars Dornheim, which contains classes for the creation, simulation and quantification of two- and three-dimensional Stable Mass-Spring Models.

All mass positions are calculated in the world coordinates system of the dataset. The associated sensors interpolate the image data dynamically to achieve subvoxel accuracy.

## 4. Results and Evaluation

To evaluate the accuracy of the model-based blood vessel reconstruction, we performed a quantitative analysis based on 30 blood vessels in 14 clinical CT datasets of the neck. The resolution of the datasets varied from 0.7 mm to 5 mm with respect to the slice distance, and between 0.3 mm to 0.8 mm in  $x$  and  $y$  direction. Among these 30 blood vessels, large and small radii were represented, as well as vessels of differing homogeneity w.r.t. the contrast agent diffusion, in order to achieve a realistic representation of typical blood vessels in the neck.

A gold standard was created for all blood vessels by segmenting the vessel with a threshold inside a rough manual contour, followed by a manual correction of over- and under-segmented areas. The resulting gold standard segmentations were verified by a radiologist.

To compare the accuracy of the model-based segmentation with the accuracy of manual segmentations, we acquired manual segmentations from two experienced users and measured their accuracy w.r.t. the gold standard. Subsequently, the results of our model adaptation were compared to the gold standard as well.

Table 2 shows that the model's accuracy w.r.t. the gold standard is comparable to the average accuracy of the users. The values for the Hausdorff distance can be attributed to large slice distances affecting the gold standard. The mean

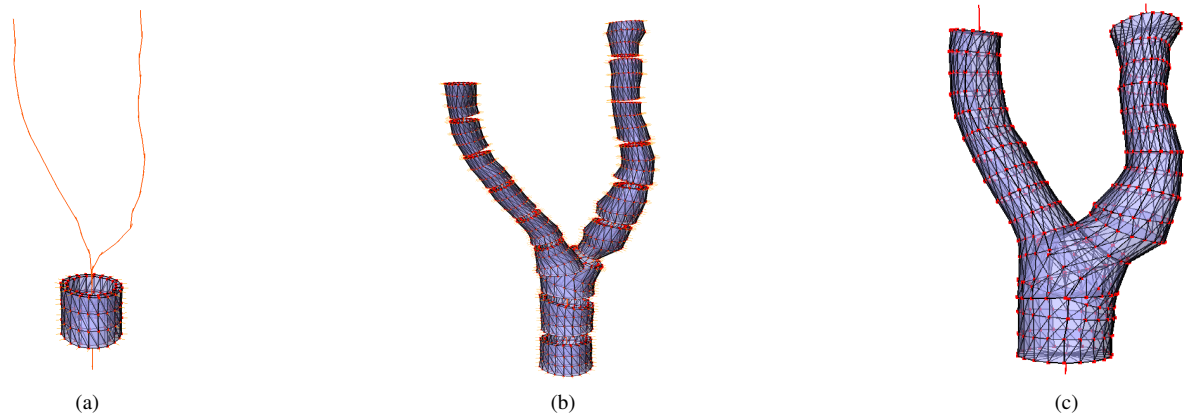


**Figure 4:** Generation of the final 3D segmentation result: (a) slicewise segmentation by the cylindrical SMSM, (b) adapted cylindrical SMSM for several slices, (c) final combination of the adapted cylindrical SMSMs for all slices

**Table 1:** Model simulation parameters (according to [DTD05])

Simulation parameter	Parameter Value
Simulation step size $\Delta t$	0.011
Tolerance (stopping criterion) $\epsilon$	0.055 mm
Max. number of simulation steps $n$	1100
Damping factor $d$	0.78

surface distance shows an accuracy of better than 1 mm. Figure 5 shows examples of successfully reconstructed blood vessels.

The average segmentation time was approximately four minutes per blood vessel on a current standard PC (Intel Pentium 4, 3.2 GHz, 1.0 GB RAM, Windows XP Professional), depending on the quality of the dataset. The interaction needed was on average 6–9 clicks per vessel, which can be carried out within 15 seconds.

## 5. Conclusions

We presented a model-based reconstruction technique for blood vessels of the neck from CT datasets, with the focus on both smooth visualizations and accuracy. The presented method enables the precise segmentation of specific vessels and ignores irrelevant branches of the vessel, independent of their size.

Due to the subvoxel accuracy of the model adaptation, the extracted blood vessels can be visualized directly without staircase artifacts, while maintaining the segmentation accuracy necessary for therapy planning and quantification. The interaction needed for the extraction could be reduced substantially from a semi-manual blood vessel segmentation to a few clicks along the vessel’s centerline. This substantial reduction of required interaction time makes the visualization

of the neck blood vessels for therapy planning feasible for the clinical routine.

Our evaluation shows that a constant set of model parameters could be determined that led to satisfying segmentation results for all examined datasets. Future work aims at a more extensive evaluation with separation of test and training data, in order to determine a generalized set of parameters. With respect to the segmentation technique, next steps include the improvement of bifurcation handling, as well as the use of an automatic measurement of the model’s successful adaptation, to detect vessel anomalies automatically.

## References

- [BKP07] BADE R., KONRAD O., PREIM B.: Reducing artifacts in surface meshes extracted from binary volumes. *Journal of WSCG 15*, 1–3 (2007), 67–74.
- [CDP\*06] CORDES J., DORNHEIM J., PREIM B., HERTEL I., STRAUSS G.: Preoperative segmentation of neck ct datasets for the planning of neck dissections. In *Proc. SPIE Medical Imaging 2006: Image Processing* (2006).
- [DSP\*07] DORNHEIM J., SEIM H., PREIM B., HERTEL I., STRAUSS G.: Segmentation of neck lymph nodes in ct datasets with stable 3d mass-spring models. *Academic Radiology (Elsevier) MICCAI 2006 Special Issue* (2007), 1389–1399.

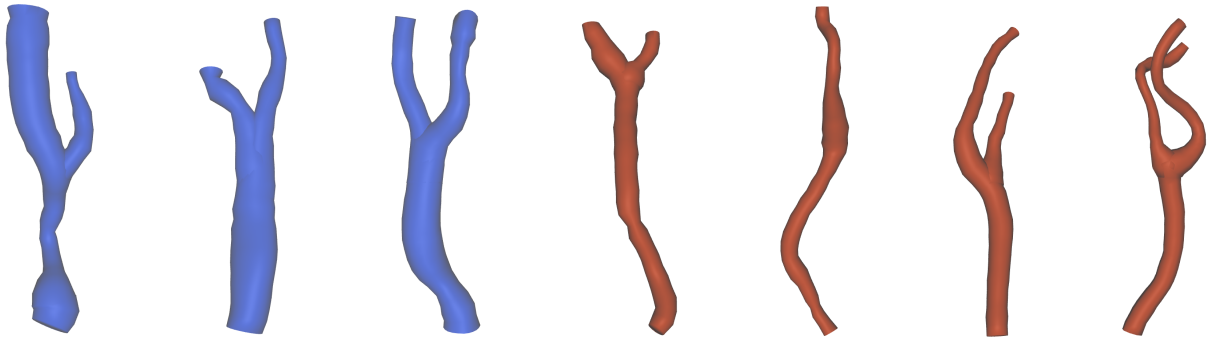


**Figure 5:** Example results of the reconstruction with SMSM (blue: V. jugularis, red: A. carotis)

**Table 2:** Results of the quantitative Evaluation

	Mean Surface Distance (mm) to gold standard	Hausdorff Distance (mm) to gold standard	Volumetric Segmentation Error w.r.t. gold standard (%)
Users ( $\bar{\sigma}$ )	0.62 ( $\sigma = 0.83$ )	8.57 ( $\sigma = 6.95$ )	0.21 ( $\sigma = 0.07$ )
Model	0.78 ( $\sigma = 0.47$ )	7.00 ( $\sigma = 6.04$ )	0.25 ( $\sigma = 0.10$ )

- [DTD05] DORNHEIM L., TÖNNIES K., DORNHEIM J.: Stable dynamic 3d shape models. In *International Conference on Image Processing (ICIP)* (2005).
- [FNN\*00] FRANGI A. F., NIESSEN W. J., NEDERKOORN P. J., ELGERSMA O. E. H., VIERGEVER M. A.: Three-dimensional model-based stenosis quantification of the carotid arteries from contrast-enhanced mr angiography. In *MMBIA '00: Proceedings of the IEEE Workshop on Mathematical Methods in Biomedical Image Analysis* (Washington, DC, USA, 2000), IEEE Computer Society, p. 110.
- [FVHO04] FLAARIS J. J., VOLDEN M., HAASE J., OSTERGAARD L. R.: Method for modelling cerebral blood vessels and their bifurcations using circular, homogeneous, generalised cylinders. *Medical and biological Engineering and Computing* 42, 2 (March 2004), 171–177.
- [Gib98] GIBSON S. F. F.: Constrained elastic surface nets: Generating smooth surfaces from binary segmented data. In *MICCAI '98: Proceedings of the First International Conference on Medical Image Computing and Computer-Assisted Intervention* (London, UK, 1998), Springer-Verlag, pp. 888–898.
- [HP03] HAHN H. K., PEITGEN H.-O.: IWT – Interactive Watershed Transform: A hierarchical method for efficient interactive and automated segmentation of multidimensional grayscale images. In *Proc. SPIE Medical Imaging 2003* (San Diego, 2003), vol. 5032, SPIE.
- [HPSP01] HAHN H. K., PREIM B., SELLE D., PEITGEN H.-O.: Visualization and interaction techniques for the exploration of vascular structures. In *IEEE Visualization* (2001), pp. 395–402.
- [KQ04] KIRBAS C., QUEK F.: A review of vessel extraction techniques and algorithms. *ACM Computing Surveys* 36, 2 (2004), 81–121.
- [MH06] MCINTOSH C., HARMANEH G.: Vessel crawlers: 3d physically-based deformable organisms for vasculature segmentation and analysis. In *IEEE Conference on Computer Vision and Pattern Recognition (CVPR)* (2006).
- [OP05] OELTZE S., PREIM B.: Visualization of vascular structures: Method, validation and evaluation. *IEEE Transactions on Medical Imaging* 24, 4 (April 2005), 540–549.
- [RTT06] RINK K., TÖRSEL A.-M., TÖNNIES K.: Segmentation of the vascular tree in ct data using implicit active contours. In *Bildverarbeitung für die Medizin (BVM)* (2006), pp. 136–140.
- [SNB\*08] SCHUMANN C., NEUGEBAUER M., BADE R., PREIM B., PEITGEN H.-O.: Implicit vessel surface reconstruction for visualization and simulation. *International Journal of Computer Assisted Radiology and Surgery (IJCARS)* 2, 5 (2008), 275–286.
- [SPSP02] SELLE D., PREIM B., SCHENK A., PEITGEN H.-O.: Analysis of vasculature for liver surgical planning. *IEEE Transactions on Medical Imaging* 21, 11 (November 2002), 1344–1357.